0026-895X/09/7503-478–489$20.00
MOLECULAR PHARMACOLOGY
Copyright © 2009 The American Society for Pharmacology and Experimental Therapeutics
Mol Pharmacol 75:478–489, 2009

Vol. 75, No. 3
50831/3438731
Printed in U.S.A.

Cu/Zn Superoxide Dismutase Typical for Familial Amyotrophic Lateral Sclerosis Increases the Vulnerability of Mitochondria and Perturbs Ca^{2+} Homeostasis in $SOD1^{G93A}$ Mice

Manoj Kumar Jaiswal and Bernhard U. Keller

Center of Physiology, Georg-August University, Goettingen, Germany

Received August 9, 2008; accepted December 4, 2008

ABSTRACT

Amyotrophic lateral sclerosis (ALS) is a fatal neurodegenerative disorder characterized by the selective loss of defined motoneuron populations in the brainstem and spinal cord. Although low cytosolic calcium ($[Ca^{2+}]_i$) buffering and a strong interaction between metabolic mechanisms and $[Ca^{2+}]_i$ have been associated with selective motoneuron vulnerability, the underlying cellular mechanisms are barely understood. To elucidate the underlying molecular events, we used rapid charge-cooled device imaging to evaluate Ca^{2+} signaling and metabolic signatures in the brainstem slices of $SOD1^{G93A}$ mice, the mouse model of human ALS, at 8 to 9 and 14 to 15 weeks of age, corresponding to the presymptomatic and symptomatic stages of motor dysfunction, respectively, and compared the results with corresponding age-matched wild-type littermates. We also monitored the mitochondrial membrane potential ($\Delta_{\Psi m}$) of brainstem motoneurons, a valuable tool for characterizing the metabolic signature of intrinsic energy profiles and considered to be a good experimental measure for monitoring energy metabolism in cells. We found that different pharmacological interventions substantially disrupt $\Delta_{\Psi m}$ in $SOD1^{G93A}$ motoneurons during the symptomatic stage. Furthermore, we investigated the impact of impaired mitochondrial mechanisms on $[Ca^{2+}]_i$ regulation by using the membrane-permeable indicator fura-acetoxy methyl ester. Taken together, the results indicate that mitochondrial disruptions are critical elements of $SOD1^{G93A}$-mediated motoneuron degeneration in which selective motoneuron vulnerability results from a synergistic accumulation of risk factors, including the disruption of electrochemical potential, low Ca^{2+} buffering, and strong mitochondrial control of $[Ca^{2+}]_i$. The stabilization of mitochondria-related signal cascades may represent a useful strategy for clinical neuroprotection in ALS.

Amyotrophic lateral sclerosis (ALS) is an adult-onset disease characterized by the degeneration of vulnerable motoneuron populations leading to paralysis and death within 5 years (Rowland and Shneider, 2001). The disease is subclassified epidemiologically as sporadic, familial, and endemic forms (Shibata, 2001), with the majority being sporadic. However, approximately 10% of cases are familial ALS (fALS) and approximately 20% of fALS cases are caused by inherited dominant mutations in the Cu/Zn-superoxide dismutase gene (*SOD1*; Rosen et al., 1993). Although the process of motoneuron degeneration in both the sporadic and familial forms is still not fully understood, researchers generally agree that there are cell-specific features impairing the mitochondrial uptake of Ca^{2+} and a low Ca^{2+} binding protein content modulating physiological and pathophysiological processes, which may render motoneurons selectively vulnerable to degeneration in ALS (Alexianu et al., 1994; Lips and Keller, 1998; Van Den Bosch et al., 2002). The loss of mitochondrial membrane potential ($\Delta_{\Psi m}$; Carrì et al., 1997), excitotoxic stimulation of AMPA/kainate receptors (Carriedo et al., 2000), and age-related motoneuron injury (Beal, 2002; Menzies et al., 2002a) may contribute to ALS pathogenesis.

Mitochondrial Ca^{2+} uptake and buffering has been associated with multiple physiological processes in motoneurons, including rhythmic activity, synaptic plasticity, and regeneration after axonal damage and has been closely linked to the

This study was supported by the Bundesministerium für Bildung und Forschung (BioRegioN/ERANET) [Grant 031 3610A]; the Bernstein Center for Computational Neuroscience Göttingen [Grant 136 2870]; and the Göttingen Center for Molecular Physiology of the Brain [Grant 135 6834].

Article, publication date, and citation information can be found at http://molpharm.aspetjournals.org.

doi:10.1124/mol.108.050831.

ABBREVIATIONS: ALS, amyotrophic lateral sclerosis; $\Delta\psi_m$, mitochondrial membrane potential; $[Ca^{2+}]_i$, cytosolic calcium; $[Ca^{2+}]_{mito}$, mitochondrial calcium; aCSF, artificial cerebrospinal fluid; AM, acetoxymethyl ester; bp, base pair(s); CCD, charge-coupled device; CPA, cyclopiazonic acid; DMSO, dimethyl sulfoxide; ER, endoplasmic reticulum; F, fluorescence; fALS, familial amyotrophic lateral sclerosis; FCCP, carbonyl cyanide *p*-(trifluoromethoxy) phenylhydrazone; hALS, human amyotrophic lateral sclerosis; HMN, hypoglossal motoneuron; PCR, polymerase chain reaction; rhod123, rhodamine 123; ROS, reactive oxygen species; RT, room temperature; SERCA, sarco-endoplasmic reticulum Ca^{2+} ATPase; SOD1, Cu/Zn superoxide dismutase 1; WT, wild-type.

regulation of electrical excitability and neurodegeneration (Bergmann and Keller, 2004; von Lewinski and Keller, 2005a; Spitzer, 2006). Excessively elevated mitochondrial Ca^{2+} ($[Ca^{2+}]_{mito}$) results in cell death by ATP depletion (Gunter and Gunter, 1994), depolarization of the $\Delta_{\Psi m}$ (Schinder et al., 1996), and subsequent generation of reactive oxygen species (ROS; Dykens, 1994). There is evidence indicating that mutated SOD1 targets mitochondria leading to structural alterations, such as mitochondrial swelling and vacuolization, in affected motoneurons (Wong et al., 1995; Kong and Xu, 1998; Menzies et al., 2002b). It has also been shown that SOD1^{G93A} inhibits complex II and IV of the mitochondrial electron transport chain leading to depolarization of the $\Delta_{\Psi m}$ and likely play a causal role in SOD1-induced motoneuron death (Mattiazzi et al., 2002). Alterations in mitochondrial electron transport, which frequently includes a decrease in complex IV, have also been found in various patients with sporadic ALS (Swerdlow et al., 1998; Borthwick et al., 1999; Vielhaber et al., 2000; Wiedemann et al., 2002).

Over the past decade, increased understanding of local interactions between Ca^{2+} and its target signaling pathways has emerged. Therefore, understanding the roles of Ca^{2+} signaling and mitochondria-mediated toxicity in ALS is crucial and of great importance. Several studies indicate that motoneuron death induced by SOD1^{G93A} involves the disruption of Ca^{2+} homeostasis; however, the underlying mechanisms are still not understood. An attractive way to investigate motoneuron function under physiological and pathophysiological conditions is to perform whole-cell, patch-clamp recordings and simultaneously monitor cytosolic signaling pathways by fluorescence microscopy (Ladewig and Keller, 2000). Previous motoneuron studies have been done on primary cultures (Carriedo et al., 2000), isolated motor nerve terminals (David et al., 2003), or by patch-clamping motoneurons in acute mouse brain slices (Ladewig et al., 2003; Bergmann and Keller, 2004). Unfortunately, the application of the patch-clamp technique to brainstem slices from adult mice is exceptionally difficult; therefore, it is important to also use alternative technical approaches. Previous attempts to use membrane-permeable forms of fluorometric calcium and membrane potential indicators to load neuron populations have worked well only in cultures or slices of neonatal brain tissue. In the current study, we attempt to introduce a robust approach for loading membrane-permeable fluorescent indicator dyes in adult brain slices and use pharmacological and fluorimetric approaches to investigate the consequences of mitochondrial inhibition on $[Ca^{2+}]_i$ and $\Delta_{\Psi m}$ in the hypoglossal motoneurons (HMNs) of adult brainstem slices. The preparation of brainstem slices from adult wild-type (WT) and corresponding SOD1^{G93A} mice is particularly valuable because it preserves motoneurons in their physiological environment in a functionally intact state and provides a way to study disease progression in a natural environment.

Materials and Methods

Transgenic Mice and PCR Genotyping. TgN (SOD1-G93A) 1Gur (Fast Line) mice were obtained from The Jackson Laboratory (Bar Harbor, ME). The Tg strain can be considered a model for human amyotrophic lateral sclerosis (hALS). The mice carry a variation of the human *SOD1* gene in which position 93 glycine is replaced by alanine (Gurney et al., 1994). These mice develop paralysis in the limbs and die at 4 to 5 months of age. This results from the continuously expanding loss of motoneurons from the brainstem and spinal cord. After the onset of symptoms, life expectancy varies from 4 to 6 weeks. Animal experiment procedures were approved and carried out in accordance with the guidelines of the ethics committee of the Medical Faculty of the University of Göttingen and met with national standards for humane care of animals. Animals were kept under a 12-h dark and light period, at 21 ± 2°C and 55 ± 10% relative humidity, were fed a standard Sniff diet (Sniff, Soest, Germany) ad libitum, and had free access to water.

PCR genotyping procedure was adapted from Hoyaux et al. (2000). The Tg male mice were bred with female B6SJL F1-hybrids obtained from The Jackson Laboratory and from Charles River Laboratories (Sulzfeld, Germany). Tg mice were identified using polymerase chain reaction. Within the first few days after birth (1–5 days), a piece of the mouse tail was dissected and 300 μl of diagnostic buffer (20 mM Tris-HCl at pH 8.4, 50 mM KCl, 0.45% Nonidet-P40, and 0.45% Tween 20) and 5 μl of Proteinase K (20 mg/ml) were added. After stirring, the process of digestion was supported by incubation for 2 h at 55°C and denaturing for 10 min at 95°C. The homogenate was then put on ice for 10 min and centrifuged at 1000*g* for 1 min. For amplification DNA (1 μl) from the digestion process, distilled water (47.5 μl), Taq PCR Master mix kit (50 μl; QIAGEN, Hilden, Germany), and special primers (0.4 μl for each primer; Sigma, Deisenhofen, Germany) were used to identify two genes: first the human *SOD1* gene on exon 4 consisting of 236 bp (primer1, oIMR114, 5′-CGC GAC TAA CAA TCA AAG TGA-3′; primer 2, oIMR113, 5′-CAT CAG CCC TAA TCC ATC TGA-3′) and second the endogenous murine *Il2* gene consisting of 324 bp (primer 3, oIMR042, 5′-CTA GGC CAC AGA ATT GAA AGA TCT-3′ and oIMR043, 5′-GTA GGT GGA AAT TCT AGC ATC ATC-3′). The *Il2* gene is used as a control for DNA amplification. The transgene carriers will amplify both genes; the wild-type samples will amplify only *Il2* gene. The amplification runs 35 cycles including 4 min at 94°C for initial denaturation, 1 min at 92°C, 1 min at 60°C, and 1 min at 72°C. Finally, the temperature is held at 72°C for 5 min and then cooled to 10°C. Ten microliters of PCR product and 5 μl of 6× loading buffer (MBI Fermantas, Vilnus, Lithuania) were run on a 2% agarose gel (80-ml tray with 7 μl of ethidium bromide dye) along with a 100-bp DNA ladder (MBI Fermantas) to estimate the size of the products.

Preparation of Acute Adult Mouse Brainstem Slices and Identification of Hypoglossal Motoneurons. Hypoglossal motoneurons (nucleus hypoglossus; XII) areas were visually identified by their proximity to the fourth ventricle while cutting the brainstem transversely (Fig. 1). In vitro brainstem slice preparations were obtained from adult (8–9 and 14–15 weeks) WT/SOD1^{G93A} mice. Animals were anesthetized with diethyl ether vapor until the paw withdrawal reflex disappeared and were then decapitated; brains were removed and subsequently cooled in 4°C cold artificial cerebrospinal fluid (aCSF). Transverse slices of the brainstem were cut with a thickness of ~200 μm using a vibroslicer (VT 1000S; Leika, Göttingen, Germany) according to a method described previously (Ladewig and Keller, 2000). To achieve maximum oxygen supply, aCSF (118 mM NaCl, 3 mM KCl, 1 mM $MgCl_2$, 25 mM $NaHCO_3$, 1 mM NaH_2PO_4, 1.5 mM $CaCl_2$, 20 mM glucose, pH 7.4; 320 mOsM) was continuously bubbled with carbogen (95% O_2/5% CO_2). An essential requirement for simultaneous microfluorometric measurements was the preservation of neurons close to the slice surface in a functionally intact state. This was achieved by minimizing mechanical disturbances of tissue during slice preparations, performing isolation of slices at low temperatures (4°C), and optimizing metabolic conditions by maximum oxygen supply. After slicing, slices were maintained at room temperature (RT, 20–23°C) for 30 min to allow recovering before dye loading. If not indicated otherwise, experiments were carried out at RT.

CCD Camera Imaging. Measurements of intracellular Ca^{2+} concentrations and mitochondrial membrane potential were performed

using a modified version of the CCD camera system (TILL Photonics, Planegg, Germany) as described previously (Lips and Keller, 1999; Ladewig and Keller, 2000). In brief, a computer-controlled monochromator based on a galvanometric scanner (Polychrome II; TILL Photonics, Martinsried, Germany) was connected to an upright microscope (Axioskope; Fa. Zeiss, Göttingen, Germany) via quartz fiber optics and a minimum number of optical components for maximum fluorescence excitation (objective Achroplan W 63×, 0.9W) was employed. Fluorescence was detected by a 12-bit CCD camera (PCO, Kelheim, Germany), binning of which was set to 4 × 4; sampling rates varied between 3 and 13 Hz. $[Ca^{2+}]_i$ changes in defined "regions of interest" drawn over the soma of motoneurons were monitored using a PC running TILL Vision Software V3.3 (TILL Photonics). The emitted light was directed to a dichroic mirror with mid reflection depending on the fluorescent dye used (fura-2 AM, 425 nm; rhod123, 510 nm; Zeiss, Germany). Switching between wavelengths was achieved in less than 3 ms, allowing rapid ratiometric Ca^{2+} measurements (for details, see von Lewinski and Keller, 2005b). Calculations and analysis of intracellular Ca^{2+} concentrations and changes in $\Delta_{\Psi m}$ were performed offline after the experiment.

Mitochondrial Membrane Potential Measurements. Rhod123 is used as an indicator of intactness of $\Delta_{\Psi m}$ (Mostafapour et al., 1997). $\Delta_{\Psi m}$ was monitored using rhod123. Adult (8–9 and 14–15 weeks) WT/SOD1^{G93A} mice brainstem slices were incubated in aCSF containing 0.5 μg/ml rhod123 at room temperature for 15 min. Slices were washed with indicator-free medium at RT for >20 min before being placed in the perfusion chamber for fluorescence analysis. Because of its positive charge, rhod123 accumulates in mitochondria, where its fluorescence is quenched. Upon depolarization of $\Delta_{\Psi m}$, rhod123 is released from mitochondria, and fluorescence increases. rhod123 was excited at 485 nm and a dichroic mirror with mid reflection at 510 was used to collect emission signal. Changes in rhod123 fluorescence are reported as relative values, F/F_0, where F_0 is the baseline fluorescence before stimulus or drug application.

Microfluorometric Ca^{2+} Measurements. Measurements of intracellular calcium concentrations were performed as described previously (Lips and Keller, 1998). Changes in the intracellular Ca^{2+} concentration ($[Ca^{2+}]_i$) were monitored using fura-2 ($K_d \sim 0.2$ μM; Invitrogen, Carlsbad, CA) after bath-loading the slices with the AM form of the dye (5 μM, 40 min at 27°C). The slices were rinsed and incubated for further 30 min in aCSF for de-esterification of fura-2 AM before onset of imaging. fura-2 was excited alternately at 360 nm and 390 nm by UV light using a computer-controlled monochromator, and emitted light was directed to a dichroic mirror with mid-reflection at 425 nm and filtered by a band-pass filter (505–530 nm; Zeiss). If not indicated otherwise, experiments were carried out at RT.

Fluorescence intensities of fura-2 were converted into Ca^{2+} concentrations according to Grynkiewicz et al. (1985), assuming K_d = 224 for HMNs (Lips and Keller, 1999; Ladewig and Keller, 2000). R_{min} and R_{max} were determined by exposing the cells to 15 μM ionomycin in the presence of aCSF containing either 0 mM Ca^{2+} and 10 mM EGTA or 10 mM Ca^{2+}. In AM-loaded slices the background fluorescence is not clearly determinable; therefore, we consider the calculated Ca^{2+} concentrations merely an approximation of the real concentration. Therefore in figures, changes in $[Ca^{2+}]_i$ are given as changes in fura-2 ratio (F/F_0), where F denotes the fluorescence values at different time points of experiment and F_0 denotes the first fluorescence value. A change of 0.1 in fura-2 ratio corresponds to a change in $[Ca^{2+}]_i$ of ~100 nM (for details, see Bergmann and Keller, 2004; von Lewinski and Keller, 2005b). Further analysis was performed offline using IGOR Pro (Wavemetrics, Lake Oswego, OR) and OriginLab (OriginLab Corp., Northampton, MA) software.

Reagents. fura-2 AM and Rhod123 was purchased from Invitrogen. Carbonyl cyanide 4-trifluromethoxyphenylhydrazone (FCCP), cyclopiazonic acid (CPA), and oligomycin were purchased from Sigma-Aldrich Chemie. Stock solutions of chemicals were prepared as follows: FCCP (10 mM) was dissolved in absolute ethanol (100%), and the stock solution was always kept at 4°C (in an ice bath) during the whole experiment to avoid ethanol evaporation. CPA (10 mg/300 μl) was dissolved in DMSO and stored as 50-μl aliquots at −20°C. Fura-2 AM (50 mg) was dissolved in 50 μl of DMSO containing 10% pluronic acid. Rhod123 (10 mg/ml) was dissolved in ethanol (100%). Oligomycin was dissolved in DMSO (5 mg/ml). The corresponding drug was then included in the perfusate and bubbled with carbogen (95% O_2/5% CO_2) at room temperature, before and during the experiments. We used 30 mM KCl for depolarization.

Statistical Analysis. Each brainstem slice was used for a single experiment and included more than one cell in fura-2 AM and rhod123 imaging experiments. In general, two slices were used from each mouse, and three or four good cells were taken from each slice for bar graph presentation. Unless indicated otherwise, values in the

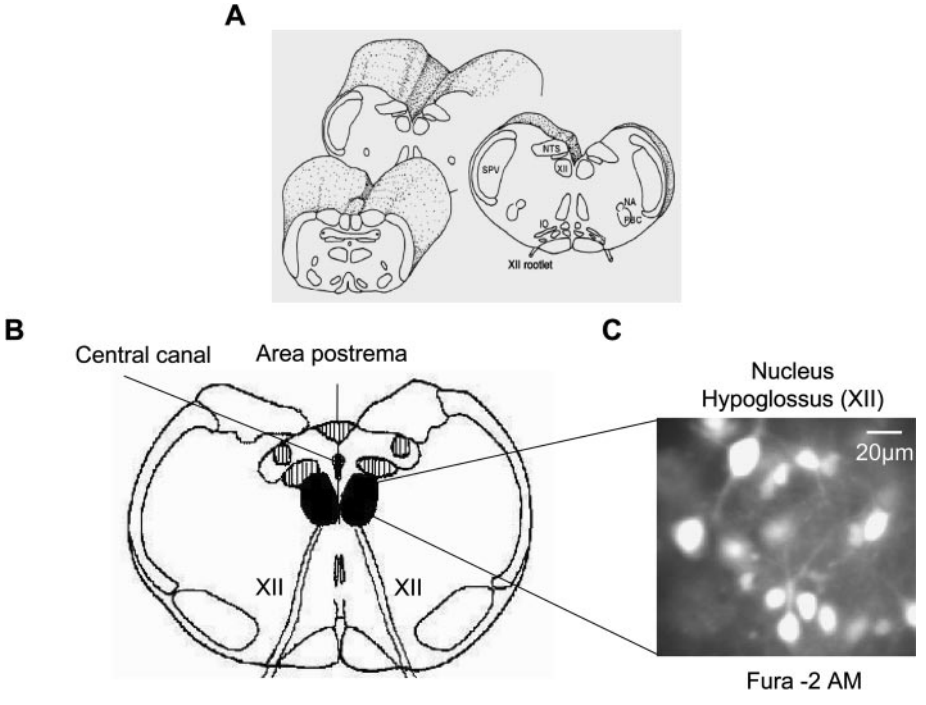

Fig. 1. Preparation of brainstem slices from WT and SOD1^{G93A} mice. A, a schematic drawing of the medulla oblongata of the isolated mouse brainstem containing the hypoglossal nucleus (XII), ambiguous nucleus (NA), pre-Bötzinger complex (PBC), solitary tract nucleus (NTS), the spinal part of the trigeminal nucleus (SPV), and the inferior olive (IO). [Modified from Ramirez JM, Quellmallz UJ, and Wilken B (1997) Developmental changes in the hypoxic response of the hypoglossus respiratory motor output in vitro. *J Neurophysiol* **78:**383–392. Copyright © 1997 American Physiological Society. Used with permission.] B, illustration of the adult mouse brainstem slice containing hypoglossal motoneurons (HMNs) marked with black colors. C, a CCD camera image (4 × 4 binning) showing HMNs loaded with rhod123 (excitation at 485 nm). Right, a CCD camera image (4 × 4 binning) showing HMNs loaded with fura-2 AM (excitation at 360 nm).

text are given as mean ± S.D. and represent at least three to five imaging experiments for at least three to five separate slices taken from individual mice. Error bars in figures represent S.D. as well. The significance after pharmacological intervention was calculated using Student's *t* test and one-way analysis of variance. Further analysis was performed off-line using IGOR and Origin software, version 7.5.

Results

Pharmacological Manipulation of Motoneuron Mitochondria by the Mitochondrial Uncoupler FCCP. To investigate the functional interplay between mitochondria and cytosolic calcium signaling, specific and rapidly acting pharmacological tools can be used. In this context, FCCP is widely used as a mitochondrial uncoupler that depolarizes the electrochemical potential by creating an ionic pore across the inner mitochondrial membrane (Billups and Forsythe, 2002; Duchen et al., 2003; Vergun et al., 2003). More specifically, FCCP is a lipophilic weak acid and therefore passes readily through surrounding cellular membranes. Besides disrupting $\Delta_{\Psi m}$, FCCP has been shown to abolish mitochondria-mediated calcium regulation and to cause the release of stored Ca^{2+} from mitochondria (Kanno et al., 2002; Feeney et al., 2003; Wyatt and Buckler, 2004; Jaiswal et al., 2006). The action of FCCP could be clearly studied based on its effect on the $\Delta_{\Psi m}$ and ensuing $[Ca^{2+}]_i$ elevation, and it did showed no nonspecific effects on cell membrane potential. The probability of FCCP localization on the plasma membrane and any resulting Ca^{2+} leak was previously checked by monitoring the current across the cell membrane in voltage-clamped HMNs; this revealed no change (Bergmann and Keller, 2004).

First, we examined the changes in the $\Delta\psi_m$ of WT and SOD1^{G93A} mice. To measure this in brainstem slices, motoneurons were loaded with rhod123, and the corresponding changes in fluorescence were monitored in the HMNs using videomicroscopic fluoroscopy (Fig. 2). The measure of the spatial heterogeneity of the rhod123 signal is sensitive to the level of mitochondrial depolarization (Toescu and Verkhratsky, 2000). In juvenile animals, HMNs display a normalized fluorescence (F/F_0) of 0.4546 ± 0.0391 and 0.4274 ± 0.0573 for WT and SOD1^{G93A} mice, respectively (Fig. 2, B and C). In essence, there were no significant differences. However, responses in adult WT animals were almost 3-fold higher compared with their SOD1^{G93A} littermates (0.3357 ± 0.0352 and 0.1106 ± 0.0406, respectively; $p < 0.001$; Fig. 2, D and E). These observations indicate that mitochondria are significantly disturbed in symptomatic SOD1^{G93A} mice.

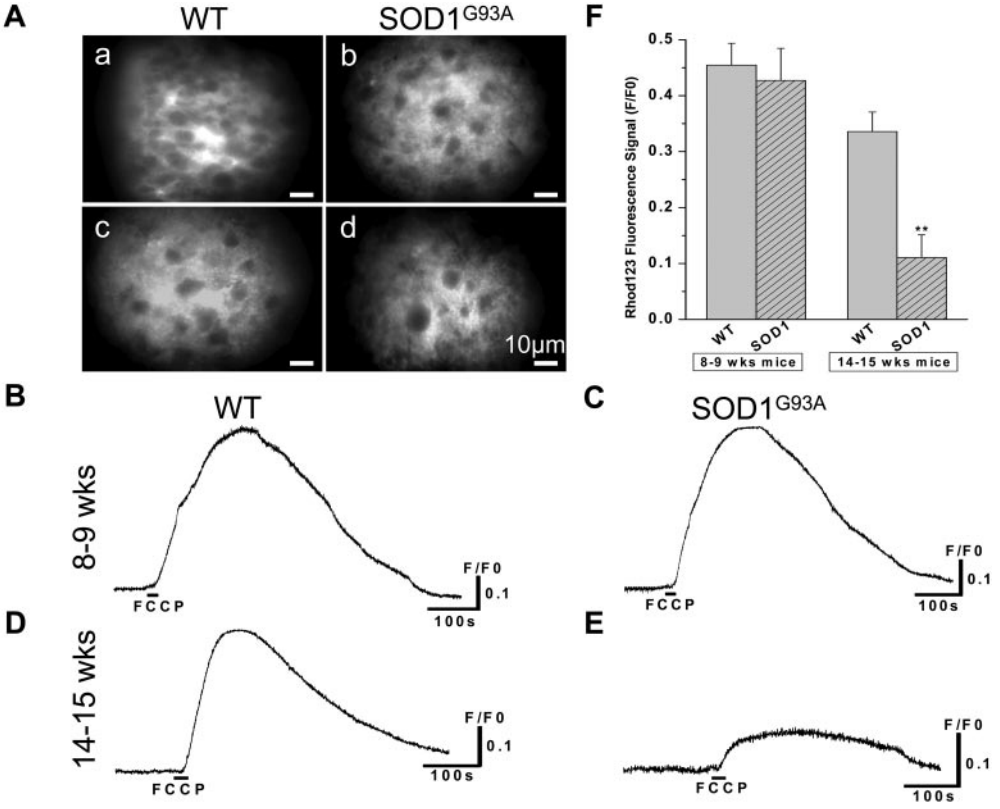

Fig. 2. Photomicrographs of rhod123-loaded brainstem slices from 8- to 9-week-old (juvenile) and 14- to 15-week-old (adult) mice and FCCP-induced mitochondrial depolarization of hypoglossal motoneurons (HMNs) in WT and SOD1^{G93A} mouse brainstem slices. A, a and b displays CCD camera images of rhod123-stained mouse brainstem slices from juvenile (presymptomatic) WT and SOD1^{G93A} mice, respectively. c and d display CCD camera images of rhod123-stained mouse brainstem slice from adult (symptomatic) WT and SOD1^{G93A} mice, respectively. The black bar indicates FCCP perfusion, which quickly released the dye quenched by mitochondria. The depolarization of HMNs juvenile WT (A) and SOD1^{G93A} mice (B) and HMNs of adult WT (D) and SOD1^{G93A} mice (E). The data represents a single cell from the brainstem slice imaged. rhod123 fluorescence signals are represented as normalized (F/F_0) values. F, bar diagram of FCCP-induced mitochondrial depolarization in the HMNs of juvenile and adult WT ($N = 3$, $n = 15$, and $n = 19$ cells, respectively) and SOD1^{G93A} ($N = 3$, $n = 13$, and $n = 17$ cells, respectively) mice. The data represent at least three separate experiments perform in separate slice for each condition and is expressed as mean ± S.D.; N = number of experiments, n = number of cells, *, $p < 0.05$; **, $p < 0.001$. The slice thickness in A is 200 μm. Scale bar, 10 μm.

Pharmacological Manipulation of Mitochondria in Motoneurons by Blocking F_1, F_0-ATP Synthase. It has been proposed that oligomycin inhibits F_1, F_0-ATPase activity by causing a conformational change in the F_0 portion of the complex that is transmitted to F_1, resulting in impaired substrate binding in the catalytic sites. Oligomycin inhibits ATP synthase by inhibiting the proton pump, thus preventing it from generating ATP. These observations of apparent conformational interactions between F_0 and F_1 on the mitochondrial membrane are relevant to the mechanism of the coupling device linking the energy store to ATP formation in oxidative phosphorylation (Stock et al., 1999).

To measure the impact of oligomycin on the $\Delta_{\Psi m}$, the brainstem slices were loaded with rhod123, and the corresponding changes in fluorescence monitored in juvenile and adult animals. Similar, but very weak, effects to those previously observed with the electron transport inhibitors (CN^-) were seen with oligomycin (Bergmann and Keller, 2004). As shown in Fig. 3, oligomycin's impact on the normalized peak of rhod123 fluorescence in juvenile animals was 0.0475 ± 0.0156 and 0.0506 ± 0.0168 for WT and $SOD1^{G93A}$ littermates, respectively (Fig. 3, A and B). Furthermore, in adult animals, normalized rhod123 fluorescence signals after oligomycin application were 0.0669 ± 0.0271 and 0.0526 ± 0.0270 for WT and $SOD1^{G93A}$ littermates, respectively ($p < 0.05$; Fig. 3, C–E).

Impact of Plasma Membrane Depolarization on Mitochondrial Function in ALS-Vulnerable Motoneurons. To determine the comparative efficiency of mitochondria upon depolarization and its influence on FCCP-evoked $\Delta_{\Psi m}$ responses, HMNs from juvenile and adult brainstem slices were challenged with FCCP after K^+ depolarization. Potassium stimulation evoked a prominent depolarization-induced mitochondrial signal. In juvenile animals, the normalized mean peak rhod123 fluorescence was 0.4123 ± 0.1104 and 0.3343 ± 0.0323 for WT and $SOD1^{G93A}$ littermates, respectively ($p < 0.05$; data not shown; quantitative values of normalized rhod123 fluorescence are compared in Table 1). However, in adult WT animals, the response was almost 2.62-fold higher compared with $SOD1^{G93A}$ littermates (0.3288 ± 0.0928 and 0.1251 ± 0.0421, respectively; Student's t test, $p < 0.001$; Data not shown; quantitative values of normalized rhod123 fluorescence are compared in Table 1). Following previous trends, there was a very small difference in the responses of juvenile mice between two genotypes. However, exposure to FCCP after a depolarizing stimulus resulted in significant differences between the responses of adult WT and symptomatic $SOD1^{G93A}$ littermates at the late stage of motor dysfunction. These observations further indicate that mitochondria are significantly disturbed in symptomatic $SOD1^{G93A}$ mice.

Impact of Plasma Membrane Depolarization and the Inhibition of F_1, F_0-ATP Synthase on FCCP-Evoked Responses of the $\Delta_{\Psi m}$. In addition to releasing various proapoptotic and toxic substances into the cytosol, mitochondrial membrane permeabilization has the potential to compromise oxidative phosphorylation. Impairment of the $\Delta_{\Psi m}$ with FCCP may block oxidative phosphorylation; in this state, glycolysis provides the primary means of ATP synthesis. The mitochondrial F_1, F_0-ATP synthase may reverse in a futile attempt to restore the $\Delta_{\Psi m}$ when depolarized by FCCP, further depleting the ATP produced via glycolysis (Budd and Nicholls, 1996). Oligomycin was added with FCCP to prevent any accelerated consumption of cellular ATP by the reverse mode of ATP synthase operation (Budd and Nicholls, 1996; Babcock et al., 1997; David et al., 1998). After plasma membrane depolarization with K^+, the mitochondrial membrane was permeabilized with FCCP and oligomycin. In juvenile animals, the HMNs displayed a normalized rhod123 fluorescence (F/F_0) of 0.7493 ± 0.0927 in WT (Fig. 4A) and 0.5501 ± 0.1903 in $SOD1^{G93A}$ (Fig. 4B, $p < 0.05$) mice, respectively. The impact of oligomycin on the peak amplitude of rhod123 fluorescence was nominal in juvenile mice, and there was no significant difference between two genotypes (0.0256 ± 0.0096 and 0.0234 ± 0.0085, respectively). However, the response to FCCP plus oligomycin in adult WT (Fig. 4C; Table 1) mice was

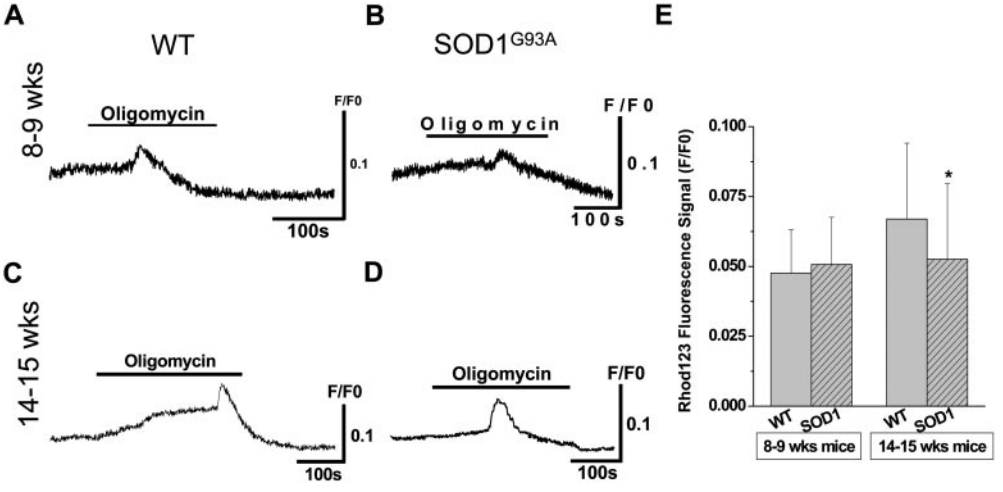

Fig. 3. Measurement of mitochondrial membrane potential ($\Delta_{\Psi m}$) in brainstem slices incubated with oligomycin to inhibit F_1, F_0-ATP synthase and deplete Ca^{2+} content. The application of 5 μg/ml oligomycin results in measurable changes in rhod123 fluorescence not only in the HMNs of 8- to 9-week-old juvenile WT (A) and $SOD1^{G93A}$ (B) mice but also in 14- to 15-week-old adult WT (C) and $SOD1^{G93A}$ (D) mice. The data represent a single cell from the slice imaged. The rhod123 fluorescence signals are represented as F/F_0. E, comparison of the peak amplitude of rhod123 signals in WT ($N = 2$, $n = 12$ and $N = 3$, $n = 18$) and $SOD1^{G93A}$ ($N = 2$, $n = 12$ and $N = 3$, $n = 18$) mice at the presymptomatic (juvenile) and symptomatic (adult) stages of motor dysfunction, respectively. The data represent at least three separate experiments for each age and each genotype and is expressed as mean ± S.D.; N = number of experiments, n = number of cells, *, $p < 0.05$.

almost 2.29-fold higher compared with SOD1^{G93A} littermates (0.3252 ± 0.0600 and 0.1416 ± 0.0316, respectively; $p < 0.001$; Fig. 4D; Table 1). The comparative details of normalized rhod123 signals in juvenile and adult animals are summarized in Fig. 4E.

Measurement of Ca^{2+} Release Responses in Motoneurons. The aim of this study was to test the role of mitochondria as a Ca^{2+} buffer under physiological conditions. Accordingly, a fura-2 AM loading protocol was established that allows for the measurement of intracellular Ca^{2+} in motoneurons without disturbing intracellular structures, which generally occurs during patch-clamp recordings. This is advantageous because, besides protecting against "washout" and the rupturing of intracellular structures, the AM loading protocol allows for the specific stereotaxic and anatomical plane of the brainstem slices that protect it from mechanical aberration and substantially preserves a large fraction of the hypoglossal nerve and neuronal network. The procedure is outlined in *Materials and Methods*. Changes in the Ca^{2+} concentration were reported as ratiometric (360/390 nm) normalized fluorescence (F/F_0).

FCCP Causes Differential Ca^{2+} Release and Ca^{2+} Transients. Blocking the mitochondrial Ca^{2+} uptake by application of FCCP for approximately 5 min has produced contrasting effects on the $[Ca^{2+}]_i$ transient and decay time constant (τ) of ALS vulnerable or resistant motoneurons (Bergmann and Keller, 2004; S. Balakrishnan and B. U. Keller, unpublished data). It was also previously found that, in HMNs and facial motoneurons, the presence of FCCP significantly delayed the τ (S. Balakrishnan and B. U. Keller, unpublished data). In the present study, there was no significant difference in the FCCP-evoked increase of $[Ca^{2+}]_i$ between the brainstem slices of juvenile WT and SOD1^{G93A} mice; the normalized peak fluorescence amplitude (F/F_0) after FCCP exposure was 0.1391 ± 0.0598 and 0.1244 ± 0.0535 for WT (Fig. 5B) and SOD1^{G93A} (Fig. 5C) littermates, respectively. The kinetics of Ca^{2+} recovery in motoneurons was also similar in juvenile mice for both genotypes. However, in adult brainstem slices, the FCCP-evoked increase in $[Ca^{2+}]_i$ was 0.1166 ± 0.0424 and 0.0533 ± 0.0316 for WT (Fig. 5D) and symptomatic SOD1^{G93A} littermates (Fig. 5E), respectively. The average mean peak fluorescence intensity is summarized in Fig. 5F.

Impact of Plasma Membrane Depolarization on Mitochondrial Ca^{2+} Uptake and $[Ca^{2+}]_i$ Release. The following pathways are responsible for the removal of Ca^{2+} from the cytosol: 1) accumulation in mitochondria, 2) sequestration in the intracellular calcium-stores of the ER, and 3) Ca^{2+} extrusion into the extracellular space by plasmalemmal Ca^{2+} pumps and/or Ca^{2+} exchangers (Pivovarova et al., 1999). Participation of all three pathways could be directly confirmed in this study by using different protocols. To analyze the comparative efficiency of mitochondria as a Ca^{2+} sequestering organelle, FCCP was applied to evacuate the

TABLE 1

Impact of plasma membrane depolarization and inhibition of F_1, F_0-ATP synthase on FCCP-evoked responses

The rhod123 fluorescence (normalized peak amplitudes F/F_0) measures mitochondrial membrane potential ($\Delta_{\psi m}$) in brainstem slices from juvenile (8–9-week-old) and adult (14–15-week-old) WT and SOD1^{G93A} mice. Data are expressed as mean ± S.D.

Rhod123 Fluorescence Unit (F/F_0)	Juvenile Mice		Adult Mice	
	WT	SOD1^{G93A}	WT	SOD1^{G93A}
Peak amplitude				
FCCP	0.4123 ± 0.1104	0.3343 ± 0.0323	0.3288 ± 0.0928	0.1251 ± 0.0421**
FCCP + oligomycin	0.7493 ± 0.0927	0.5501 ± 0.1903	0.3252 ± 0.0600	0.1416 ± 0.0316**

** $p < 0.001$ compared with WT.

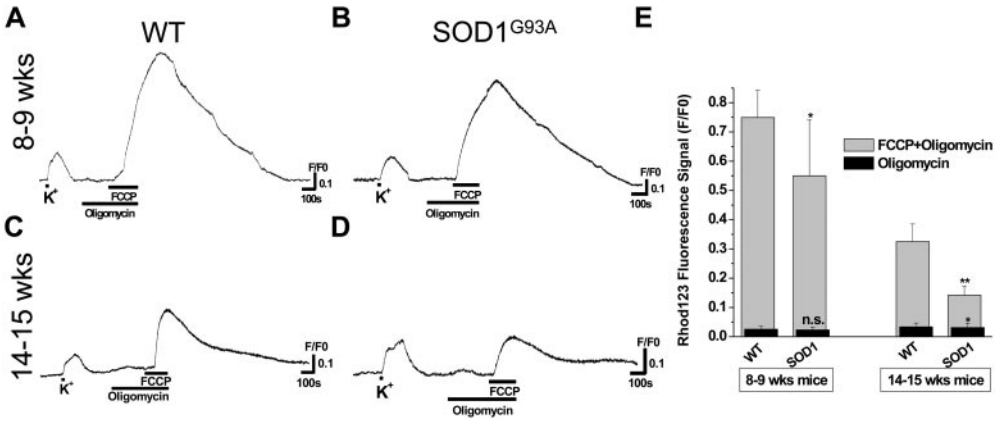

Fig. 4. Impact of plasma membrane depolarization and inhibition of F_1, F_0-ATP synthase on FCCP-evoked responses of the mitochondrial membrane potential ($\Delta_{\Psi m}$) in brainstem slices of juvenile (8–9-week-old) and adult (14–15-week-old) mice. Rhod123 fluorescence after stimulation-evoked $\Delta_{\Psi m}$ before and after application of oligomycin and FCCP in juvenile WT (A) and SOD1^{G93A} (B) mice and adult WT (C) and SOD1^{G93A} (D) mice. The horizontal black bars indicate the duration of K^+ induced plasma membrane depolarization, stimulation with oligomycin, and stimulation with FCCP, respectively. E, a graphical representation of the effect of oligomycin alone and oligomycin plus FCCP on the $\Delta_{\Psi m}$ in juvenile ($N = 3$) and adult ($N = 3$) WT ($n = 10$ and n = 21, respectively) and SOD1^{G93A} ($n = 12$ and $n = 17$, respectively) mice. Note that the $\Delta_{\Psi m}$ is not significantly affected by oligomycin in any of the mice, but that FCCP exhibits an increased rhod123 signal that is significantly diminished in symptomatic (adult) SOD1^{G93A} mice (**, $p < 0.001$) compared with WT littermates (2.26-fold). Small differences in the rhod123 signals of juvenile mice (*, $p < 0.05$) were also noted. The data are expressed as mean ± S.D.; N = number of experiments, n = number of cells. The data represent at least three separate experiments for each age and each genotype in separate slices.

mitochondria after the cells were exposed to a Ca^{2+} load evoked by a depolarizing stimulus, K^+. When motoneurons were exposed to 30 mM K^+ for 20 s, the $[Ca^{2+}]_i$ increased rapidly and subsequently returned to the basal level, whereas mitochondria and ER retained large pools of Ca^{2+}, presumably for later extrusion from the cell. To determine whether the mitochondrial accumulation of Ca^{2+} has any apparent influence on the lifetime of the $[Ca^{2+}]_i$ transient, and to test whether a large Ca^{2+} pool exists, FCCP was added to the superfusate after K^+-induced depolarization. In the case of juvenile brainstem slices, the application of FCCP within 5 min of depolarization induced by K^+ resulted in a calcium release measured by the fura-2 fluorescence ratio (F/F_0) of 0.1478 ± 0.0426 and 0.1312 ± 0.0468 for WT and $SOD1^{G93A}$ littermates, respectively (data not shown; quantitative fluorescence value compare in Table 2). However, following previous trends there was a slight increase in the fluorescence after cell membrane depolarization compared with the fluorescence before depolarization (Fig. 5, B and C), but there was no significant difference in the FCCP-evoked responses (normalized, F/F_0) between two genotypes. A similar application of FCCP in adult brainstem slices resulted in a Ca^{2+} release of 0.1416 ± 0.0458 and 0.0619 ± 0.0269 (F/F_0) for WT and $SOD1^{G93A}$ animals, respectively (Data not shown; quantitative fluorescence value compare in Table 2). This implies that there is a significant difference between the motoneurons of WT and $SOD1^{G93A}$ mice at the late stage of motor dysfunction in the Ca^{2+} accumulation activity of mitochondria.

Pharmacological Manipulation of ER in Motoneurons by CPA Inhibition of SERCA and Its Impact on Differential Ca^{2+} Store Regulation. The ER functions as an effective Ca^{2+} storing organelle. The active transport of $[Ca^{2+}]_i$ into intracellular stores by sarco-endoplasmic reticulum Ca^{2+}-ATPase (SERCA) is important in regulating Ca^{2+} signaling (Cavagna et al., 2000). Moreover, inhibition of Ca^{2+} uptake by the ER has been shown to disrupt Ca^{2+} homeostasis (Trump and Berezesky, 1995). To test whether the ER serves either of these roles in the motoneurons, we measured the calcium release from the ER in the presence of CPA, a specific inhibitor of the SERCA family of pumps (Simpson and Russell, 1997). The application of CPA evoked a rise in the $[Ca^{2+}]_i$ transient (Fig. 6), which is indicative of Ca^{2+} leakage from the intracellular Ca^{2+} stores. The treatment caused a gradual release of Ca^{2+} from ER stores at basal condition and was recorded in both WT and $SOD1^{G93A}$ mice brainstem slices for both juvenile and adult animals. The Ca^{2+} release (F/F_0) in juvenile mice was 0.0857 ± 0.0382 and 0.0667 ± 0.0135 in WT and $SOD1^{G93A}$ littermates, respectively (Fig. 6, A and B). In adult mice, the release of Ca^{2+} (F/F_0) was 0.0817 ± 0.0332 and 0.0542 ± 0.0202 in WT and $SOD1^{G93A}$ littermates, respectively (Fig. 6, C and D). In these experiments, the application of CPA resulted in more or less identical Ca^{2+} release responses, although in adult $SOD1^{G93A}$ brainstem slices, these values are slightly lower ($p < 0.05$; Student's t test and one-way analysis of variance). The comparison of average HMN ER calcium release in juvenile and adult animals of different genotypes is presented in Fig. 6E.

Interaction between ER and Mitochondria in Differential Ca^{2+} Store Regulation and the Role of the ER As a Ca^{2+} Sequestering Organelle. Evidence is building regarding the reciprocal functional interplay between the ER and mitochondria in response to various toxic agents in ALS, Alzheimer's, and Parkinson's disease (Paschen and Mengesdorf, 2005). It was previously shown in *Caenrhabditis elegans* that high intracellular Ca^{2+} levels and the release of ER-based Ca^{2+} stores are essential steps in the necrotic death mechanism of neurons (Xu et al., 2001). Furthermore, Ca^{2+}

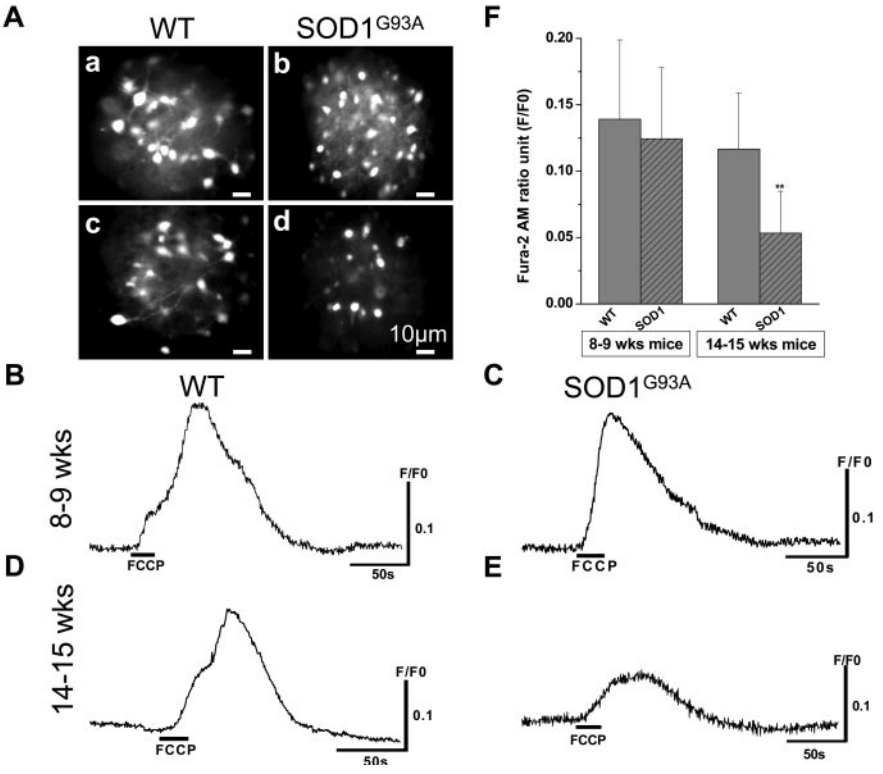

Fig. 5. The impact of FCCP on differential cytosolic calcium ($[Ca^{2+}]_i$) release in juvenile (8–9-week-old) and adult (14–15-week-old) WT and $SOD1^{G93A}$ mice. A, photomicrographs of fura-2 AM-loaded brainstem slices (200 μm) in juvenile (a and b) and adult (c and d) WT (a and c) and $SOD1^{G93A}$ (b and d) mice. The black bar indicates perfusion with FCCP, which quickly facilitates $[Ca^{2+}]_i$ release in the hypoglossal motoneurons (HMNs) of juvenile WT (B) and $SOD1^{G93A}$ mice (C), and adult WT (D) and $SOD1^{G93A}$ mice (E). The data represent a single cell from the slice imaged. F, a bar diagram of FCCP-induced $[Ca^{2+}]_i$ release in the HMNs of juvenile and adult WT ($N = 3$; $n = 14$ and $n = 24$, respectively) and $SOD1^{G93A}$ ($N = 3$; $n = 14$ and $n = 21$, respectively) mice. The fura-2 AM signal is represented as F/F_0. The data represent at least three independent experiments for each genotype and is expressed as mean ± S.D.; N = number of experiments, n = number of cells. **, $p < 0.001$. Scale bar, 10 μm. The data represent at least three separate experiments for each age and each genotype in separate slices

release from the ER contributes to neuronal cell death because the Ca^{2+} release blocker, dantrolene, can protect neurons against bioenergetic failure and cellular damage (Wei and Perry, 1996). If this is true, the restoration of ER function or attenuation of the secondary dysfunction induced by ER could present a new, highly promising avenue for pharmacological intervention to minimize neuronal cell injury in the pathological states of ALS.

A comparative analysis of the Ca^{2+} storing ability of mitochondria and ER in juvenile and adult brainstem slices was done using FCCP and CPA. There was a significant quantitative difference between the ER and mitochondrial Ca^{2+} load in the case of healthy and ALS-vulnerable HMNs at the late stage of motor dysfunction; the Ca^{2+} release response was high in the mitochondria of WT mice. As shown in Fig. 7, in juvenile mice, the peak amplitude of mitochondrial Ca^{2+} release after application of FCCP plus CPA was 0.1738 ± 0.04659 and 0.1792 ± 0.0654 in WT and SOD1^{G93A} littermates, respectively (Fig. 7, A and B; Table 2). The impact of CPA on the peak amplitude of Ca^{2+} release was nominal compared with FCCP, indicating a lesser role for ER compared with mitochondria in Ca^{2+} storage, as exemplified by juvenile WT and SOD1^{G93A} mice (0.0342 ± 0.0087 and 0.0335 ± 0.0111, respectively; Fig. 7, A and B; Table 2). In adult mice, the peak amplitude of $[Ca^{2+}]_i$ after CPA application was 0.0497 ± 0.0245 and 0.0311 ± 0.0087 for WT and SOD1^{G93A} littermates, respectively ($p < 0.05$), whereas the response to FCCP plus CPA was 0.2095 ± 0.0695 and 0.0967 ± 0.0284 for WT and SOD1^{G93A} littermates, respectively ($p < 0.001$; Fig. 7, C and D; Table 2). Comparative details of the normalized fura-2 ratio in juvenile and adult animals are summarized in Fig. 7E.

Discussion

When rhod123-loaded HMNs were treated with FCCP, there was a sudden and reversible increase in fluorescence, indicating the transient loss of $\Delta_{\Psi m}$. An increased response to FCCP in WT compared with SOD1^{G93A} mice, which are at the symptomatic stage of motor dysfunction, supports the hypothesis that mitochondrial Ca^{2+} homeostasis is significantly disturbed in SOD1^{G93A} mice and that mitochondria play a crucial role in motoneuron degeneration in the mouse model of hALS-fALS. Furthermore, we compared the efficiency of depolarization-induced mitochondrial responses after stimulation with K^+. Again, FCCP-evoked responses were significantly smaller in adult SOD1^{G93A} compared with WT mice, suggesting impaired mitochondria.

We would expect that the ATP available for cellular processes, such as membrane Ca^{2+} ATPases, would be lowest during bath application of FCCP. We found that bath application of oligomycin alone results in the inhibition of ATP via oxidative phosphorylation, and the $\Delta_{\Psi m}$ remains intact because of the reduction, but not depletion, of cellular ATP as a result of glycolysis. Under physiological conditions, mitochondrial uptake of calcium may occur via the calcium uniporter supported by the intact electrochemical gradient. However, oligomycin did not cause any significantly different postdepolarization and basal $[Ca^{2+}]_i$ regulation in either juvenile or adult WT and SOD1^{G93A} littermates. These results

TABLE 2

Differential peak amplitudes of Ca^{2+} release from endoplasmic reticulum and mitochondria in brainstem slices from juvenile (8–9-week-old) and adult (14–15-week-old) WT and SOD1^{G93A} mice

Data are expressed as mean ± S.D.

Fura-2 AM Ratio Unit (F/F_0)	Juvenile Mice		Adult Mice	
	WT	SOD1^{G93A}	WT	SOD1^{G93A}
Ca^{2+} peak amplitude				
FCCP	0.1478 ± 0.0426	0.1312 ± 0.0468	0.1416 ± 0.0458	0.0619 ± 0.0269**
FCCP + CPA	0.1738 ± 0.0466	0.1792 ± 0.0654	0.2095 ± 0.0695	0.0967 ± 0.0284**

** $p < 0.001$ compared with WT.

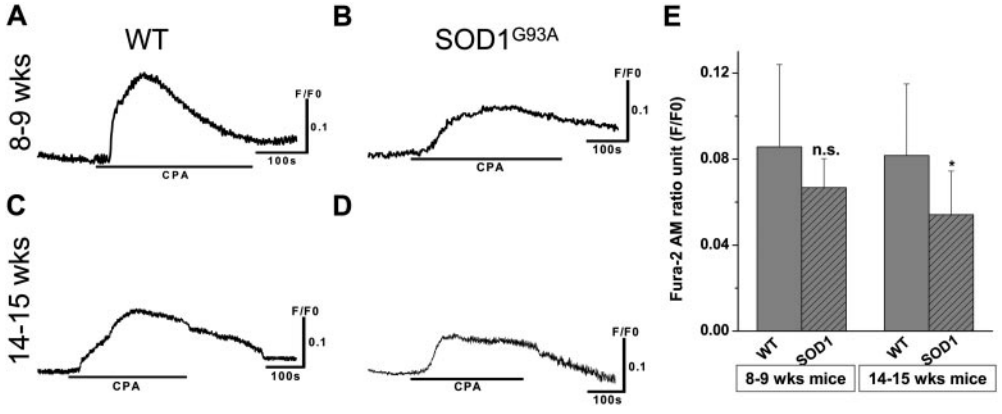

Fig. 6. Differential Ca^{2+} store regulation in the ER of juvenile and adult WT and SOD1^{G93A} mice. Brainstem slices were incubated with CPA to inhibit ER Ca^{2+}-ATPase and thereby deplete the Ca^{2+} content. The application of 50 μM CPA resulted in measurable Ca^{2+} release from the HMNs of juvenile WT (A) and SOD1^{G93A} mice (B), and adult WT (C) and SOD1^{G93A} (D) mice. The data represent a single cell from the slice imaged. Fura-2 AM signals are represented as F/F_0. E, comparison of the amplitude of the ER calcium release in these motoneurons as a result of SERCA pump inhibition; the data represent at least three independent experiments ($N = 3$; $n = 12$) for each genotype. Data are expressed as mean ± S.D.; N = number of experiments, n = number of cells. *, $p < 0.05$.

indicate that, in contrast to FCCP, blockade of the mitochondrial F_1, F_0-ATP synthase by oligomycin is associated only with a minor impact on $\Delta_{\Psi m}$ without discrimination of genotype or age. It was also noted that the reverse F_1, F_0-ATP synthase cycle or restoration of $\Delta_{\Psi m}$ (Budd and Nicholls, 1996) was very rare and more likely to occur in adult SOD1^{G93A} Tg mice. This could be due to several factors, including aging, vulnerable motoneurons, and the slow activity of the mitochondrial Na^+/Ca^{2+} exchanger.

The Impact of Mitochondrial Disruption on Ca^{2+} Uptake and Release. Our interest in studying the role of Ca^{2+} regulation and the impact of mitochondrial inhibition on HMNs is based on several observations that mitochondria act as local calcium buffers, thus shaping the spatiotemporal aspects of $[Ca^{2+}]_i$ signals. Mitochondria in HMNs and facial motoneurons have a major percentage of cellular Ca^{2+} sequestered intracellularly after influx through the plasma membrane (Balakrishnan et al., 2004). In juvenile mice, we found no difference in the FCCP-evoked $[Ca^{2+}]_i$ increase between two genotypes. However, the FCCP-evoked mitochondrial Ca^{2+} release responses (normalized) in WT adult mice were of a greater amplitude and substantially more prominent than those in corresponding SOD1^{G93A} littermates. In the HMNs of adult SOD1^{G93A} mice, mitochondrial Ca^{2+} release was much less after the preceding $[Ca^{2+}]_i$ increase. These data indicate that the processes responsible for the release of $[Ca^{2+}]_i$ are qualitatively different in adult WT and SOD1^{G93A} mice. The main difference in the mitochondrial function of adult WT and SOD1^{G93A} mice is their capability to accumulate a large amount of Ca^{2+} in rapidly in the motoneurons of WT mice compared with the delayed accumulation of much smaller amounts in SOD1^{G93A} mice. The higher load of calcium in the HMNs of juvenile WT/SOD1^{G93A} mice and adult WT mice can be attributed to the specialization of these cells to obtain Ca^{2+}. This specialized property of HMN mitochondria could be vital in ALS pathology as the high glutamate concentration in synapses can lead to massive cellular entry and overaccumulation of $[Ca^{2+}]_{mito}$, which is a conventional trigger for mitochondrial swelling and permeability transition. Under such circumstances, the HMNs of SOD1^{G93A} mice in which the mitochondria buffer Ca^{2+} are at particular risk compared with other motoneurons, which are supplied with an abundance of Ca^{2+}-chelating proteins. This supports the model that $[Ca^{2+}]_{mito}$ homeostasis is significantly altered in SOD1^{G93A} mice at the symptomatic stage of motor dysfunction.

It has already been shown that the application of FCCP alone, without predepolarization, induces only small $[Ca^{2+}]_i$ elevations in motoneurons. However, if FCCP is applied immediately after the termination of depolarization during the decay of the induced transient, FCCP causes a large release of Ca^{2+}, demonstrating the effectiveness of the immediate uptake of Ca^{2+} into the cell through plasmalemmal channels (S. Balakrishnan and B. U. Keller, unpublished data). In this study, FCCP was applied for a longer interval after the termination of depolarization. We observed that, when Ca^{2+} returns to its basal level, it produces only a very small $[Ca^{2+}]_i$ increase, although the Ca^{2+} store was approximately 2.28-fold greater in adult WT mice compared with SOD1^{G93A} mice. The excess Ca^{2+} that emerges in the second response seems to be hidden by the mitochondrial uptake of the first response. This data can be explained two ways: 1) there is a progressive leak of ions from the mitochondria back into the cytosol and/or 2) Ca^{2+} homeostasis is significantly disturbed in vulnerable SOD1^{G93A} motoneurons, and mitochondria have a lower capacity to store Ca^{2+} released by depolarization. Therefore, we conclude that the mitochondria in adult WT motoneurons are capable of retaining Ca^{2+} for a longer time compared with vulnerable SOD1^{G93A} motoneurons. The experiments also indicated that mitochondria contribute to the fast clearance of Ca^{2+} transients by taking up approximately 50% of the motoneuron Ca^{2+} loads, even for small $[Ca^{2+}]_i$ elevations (50–200 nM, physiological range; S. Balakrishnan and B. U. Keller, unpublished observations). This is evident with the FCCP prevention of mitochondrial contributions to Ca^{2+} uptake, resulting in a severe delay in the $[Ca^{2+}]_i$ transient recovery time in symptomatic SOD1^{G93A} mice.

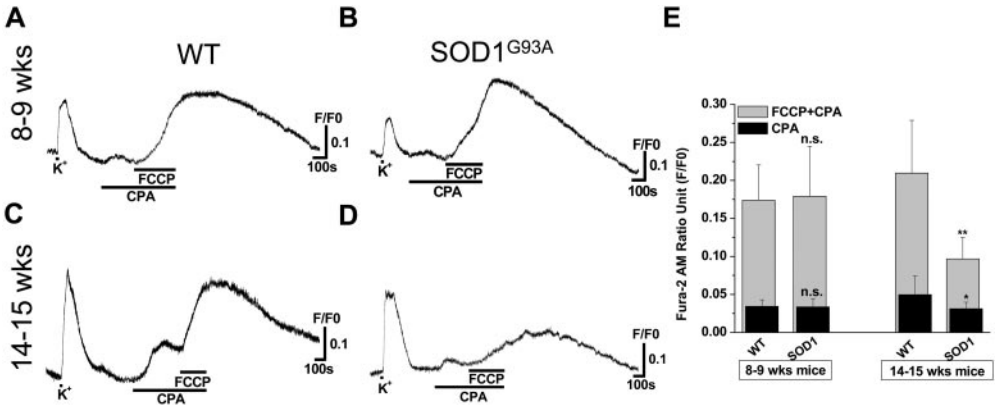

Fig. 7. Comparative analysis of the differential Ca^{2+} storage and regulation of the ER and mitochondria in juvenile and adult WT and SOD1^{G93A} mice. The HMNs in brainstem slices were stimulated using FCCP and CPA, which interfere with the integrity of the mitochondria and ER, respectively, and were used to release quenched calcium. Quantitative differences were evident in juvenile WT (A) and SOD1^{G93A} mice (B), as well as adult WT (C) and SOD1^{G93A} (D) mice. The horizontal black bars indicate the duration of K^+ induced depolarization, stimulation by CPA, and stimulation with FCCP plus CPA, respectively. The data represent a single cell from the slice imaged. Fura-2 AM signals are represented as F/F_0. E, a graphical representation of the comparison of Ca^{2+} release from the ER and mitochondria in HMNs from 8- to 9-week- and 14- to 15-week-old mice ($N = 3$) after application of CPA or CPA plus FCCP ($n = 13$). The data represent at least three independent experiments ($n = 13$) for each genotype and is expressed as mean ± S.D.; N = number of experiments, n = number of cells, **, $p < 0.001$; *, $p < 0.05$.

Interaction of Mitochondrial Ca^{2+} Stores with the Endoplasmic Reticulum. Different intracellular pools participate in the generation of Ca^{2+} signals in neuronal cells, shaping their spatiotemporal patterns and the cell life-death cycle (Herrington et al., 1996; Schinder et al., 1996). We found that the ER of HMNs retained a low amount of calcium compared with mitochondria after $[Ca^{2+}]_i$ elevation, indicating its low efficiency at sequestering Ca^{2+} in the HMNs of adult WT and SOD1^{G93A} mice, which was slightly higher in juvenile mice. This indicates that the conventional mitochondrial Ca^{2+} storing function dominates ER Ca^{2+} accumulation in these motoneurons. It is noteworthy that CPA has a relatively weak effect on Ca^{2+} release in symptomatic SOD1^{G93A} mice, indicating that SOD1^{G93A} mutations might also result in defects in ER Ca^{2+} handling, which may perturb synaptic function and contribute to neurodegeneration. These data suggest that the ER of HMNs does not play a significant role in regulating $[Ca^{2+}]_i$ at the basal level or after imposed Ca^{2+} loads in juvenile WT or SOD1^{G93A} mice. However, in adult mice, during ALS progression, the ER does contribute some to the dysfunction of Ca^{2+} loads, suggesting that Ca^{2+} dysregulation as a result of the SOD1^{G93A} mutation is a late-onset event and anticipates ALS progression.

The application of FCCP to CPA on HMNs clearly caused a separate Ca^{2+} release response. In adult WT HMNs, the ER Ca^{2+} release was slightly more than in SOD1^{G93A} mice, indicating that, in the context of the SOD1^{G93A} mutation, the ER may contribute at the late stage of motor dysfunction. Furthermore, the application of FCCP after emptying ER stores with CPA resulted in a separate release event, evident from the $[Ca^{2+}]_i$ increase. This release was higher than the general Ca^{2+} release caused by FCCP without emptying ER in juvenile WT and SOD1^{G93A} mice, but not in adult SOD1^{G93A} mice, which suggests an uptake of the released Ca^{2+} from ER by mitochondria in juvenile mice. This further indicates the explicit action of FCCP in our working model system and the existence of two separate intracellular Ca^{2+} stores, in which the ER seems to play a minimal role in buffering $[Ca^{2+}]_i$ after Ca^{2+} loads are imposed on the HMNs of SOD1^{G93A} mice, and the ER is most likely not impaired during ALS-related motoneuron disease. Our hypothesis is strengthened by the fact that we previously obtained similar

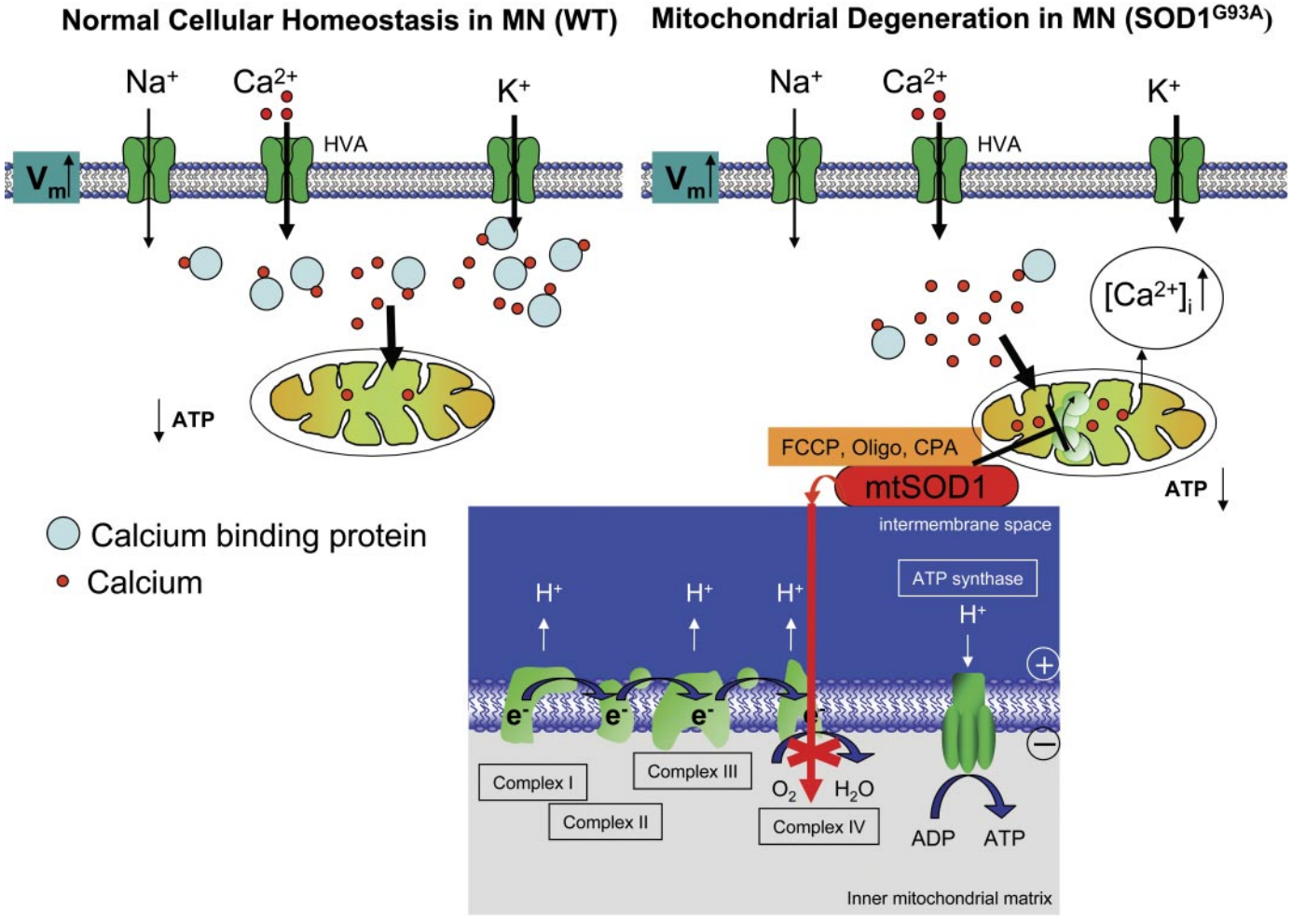

Fig. 8. Pathological mechanisms in ALS: a differential functional model of interactions between mitochondria and high Ca^{2+} levels. The compound FCCP selectively depolarizes hypoglossal motoneurons and increase their $[Ca^{2+}]_i$ load in vulnerable motoneurons. Events after the mitochondrial inhibition inhibit complex IV of the electron transport chain, which leads to ROS generation. The inhibition of the respiratory chain further decreases the $\Delta_{\Psi m}$, leading to reduced Ca^{2+} uptake into the mitochondrial matrix and the release of Ca^{2+} taken up during preceding activity. The risk becomes much higher when mitochondria are placed cardinally to buffer the calcium and control the subsequent metabolic pathways as an uncontrolled elevation in $[Ca^{2+}]_i$ can lead to immediate cell death. Mitochondrial inhibition additionally decreases cellular ATP levels, and this further enhances accumulation of $[Ca^{2+}]_i$. The observed changes provide a potential mechanism of how mitochondrial inhibition can lead to selective motoneuron degeneration.

results in a cell culture model of WT-SOD1 and $SOD1^{G93A}$ transfected SH-SY5Y cells. Caffeine selectively blocked Ca^{2+} uptake into the ER and mitochondrial compartments and affected its release from intracellular storage sites. The ryanodine receptor led to a relatively slow and weak increase of $[Ca^{2+}]_i$ and $[Ca^{2+}]_{mito}$, which occurred with slightly higher kinetics in WT cells than the $SOD1^{G93A}$ transfected cells (M. K. Jaiswal, W.-D. Zech, M. Goos, C. Leutbecher, A. Ferri, A. Zippelius, M. T. Carrí, R. Nau, and B. U. Keller, unpublished data). This explains that ER-dependent Ca^{2+} release is a minor contribution to mitochondria-mediated toxicity in $SOD1^{G93A}$ HMNs as previously reported in other cell types and animal models (Murayama et al., 2000; Fill and Copello, 2002; Sher et al., 2007). This could indicate close coupling between these two organelles in healthy motoneurons. The results also indicate that, with ALS progression, close coupling between the ER and mitochondria is impaired.

Our results are in agreement with the "hotspot hypothesis" that mitochondria preferentially accumulate Ca^{2+} at microdomains of elevated $[Ca^{2+}]_i$ that exist near ER Ca^{2+} release sites and other Ca^{2+} channels. Accordingly, mitochondria may affect both Ca^{2+} release from the ER and capacitative Ca^{2+} entry across the plasma membrane, thereby shaping the size and duration of the $[Ca^{2+}]_i$ signal in the HMNs of WT and $SOD1^{G93A}$ mice and the recruitment of these signals for selective motoneuron degeneration. The molecular mechanisms defining the organization of mitochondria in murine motoneurons with regard to the ER and other Ca^{2+} sources, and the extent to which mitochondrial function varies among different cell types, are questions that remain unanswered but are interesting areas for future investigations.

Potential Impact for Future Neuroprotective Strategies. The vulnerability of HMNs in ALS raises many questions, and the evident mitochondrial pathological lesions observed in patients with ALS and animal models suggest a central role for the degradation of mitochondrial integrity and metabolism by uncontrolled $[Ca^{2+}]_{mito}$ accumulation leading to a vicious circle of pathological mechanisms finally transformed into a fatal cycle (Fig. 8). Given the mitochondrial disturbances, Ca^{2+} buffering becomes inefficient and cytosolic Ca^{2+} levels rise. The protective option is to increase the resistance of motoneurons to high intracellular Ca^{2+} concentrations by inducing defense mechanisms and/or to inhibit the downstream pathways activated by increased $[Ca^{2+}]_i$. However, severely impaired HMNs are prevented from taking advantage of neuronal protection, including a more defined separation of spatial Ca^{2+} gradient signal cascades. Moreover, recent research indicates that therapeutic options do not have to focus on motoneurons alone, because ALS seems to be a more intricate disease also involving glia, astrocytes, muscle, and in some cases inflammation and apoptosis. In conclusion, it seems that ALS is a multifactorial disease in which, under physiological conditions, diffusion-restricted and tightly controlled domains might indeed have several functional advantages. Accordingly, therapeutic measures aimed at protecting mitochondrial function could be useful in various forms of ALS. However, the surprisingly similar pathological nature of motoneuron degeneration in different forms of ALS provides an ongoing challenge to integrate the different aspects in a more unifying scheme. In this context, our results indicate that $\Delta_{\Psi m}$, the inhibition of mitochondrial respiratory chain and energy production, and specialized Ca^{2+} homeostasis in motoneurons accounts for versatile and dynamic Ca^{2+} signaling and are critical in ALS pathophysiology. They are also associated with a number of ALS-related risk factors, including low buffering, the important role of mitochondria in regulating $[Ca^{2+}]_i$ and the presence of large and long-lasting Ca^{2+} domains. It is conceivable that a combination of therapies addressing the many intercellular targets in ALS could be successful at treating this once-obscure disease, although it is clear that more structural and functional studies are currently needed to identify potential cytosolic pathways and barriers leading to motoneuron degeneration in ALS. Forthcoming studies could add to the understanding of why these processes preferentially damage motoneurons and the function of non–cell-autonomous cell death (glia and astrocytes), if any. Taken together, our observations support the notion that mitochondria significantly enhance the selective vulnerability of motoneurons in hALS and corresponding mouse models.

Acknowledgments

We thank D. Crzan and Cornelia Hühne for excellent technical assistance and Drs. Saju Balakrishnan, Friederike von Lewinski, Michael Müller, Eike Schomburg, and Diethelm Richter for valuable discussions.

References

Alexianu ME, Ho BK, Mohamed AH, La Bella V, Smith RG, and Appel SH (1994) The role of calcium-binding proteins in selective motoneuron vulnerability in amyotrophic lateral sclerosis. *Ann Neurol* **36:**846–858.

Babcock DF, Herrington J, Goodwin PC, Park YB, and Hille B (1997) Mitochondrial participation in the intracellular Ca^{2+} network. *J Cell Biol* **136:**833–844.

Balakrishnan S, Bergmann F and Keller BU (2004) Mitochondria differentially regulate $[Ca]_i$ in brainstem motoneurons from mouse: implications for selective motoneuron vulnerability. *Soc Neurosci Abstr* **30:**508.8.

Bergmann F and Keller BU (2004) Impact of mitochondrial inhibition on excitability and cytosolic Ca^{2+} levels in brainstem motoneurons from mouse. *J Physiol* **555:**45–59.

Beal MF (2002) Oxidatively modified proteins in aging and disease. *Free Radic Biol Med* **32:**797–803.

Billups B and Forsythe ID (2002) Presynaptic mitochondrial calcium sequestration influences transmission at mammalian central synapses. *J Neurosci* **22:**5840–5847.

Borthwick GM, Johnson MA, Ince PG, Shaw PJ, and Turnbull DM (1999) Mitochondrial enzyme activity in amyotrophic lateral sclerosis: implications for the role of mitochondria in neuronal cell death. *Ann Neurol* **46:**787–790.

Budd SL and Nicholls DG (1996) Mitochondria, calcium regulation, and acute glutamate excitotoxicity in cultured cerebellar granule cells. *J Neurochem* **67:**2282–2291.

Carrì MT, Ferri A, Battistoni A, Famhy L, Gabbianelli R, Poccia F, and Rotilio G (1997) Expression of a Cu,Zn superoxide dismutase typical of familial amyotrophic lateral sclerosis induces mitochondrial alteration and increase of cytosolic Ca^{2+} concentration in transfected neuroblastoma SH-SY5Y cells. *FEBS Lett* **414:**365–368.

Carriedo SG, Sensi SL, Yin HZ, and Weiss JH (2000) AMPA exposures induce mitochondrial Ca^{2+} overload and ROS generation in spinal motor neurons in vitro. *J Neurosci* **20:**240–250.

Cavagna M, O'Donnell JM, Sumbilla C, Inesi G, and Klein MG (2000) Exogenous Ca^{2+}-ATPase isoform effects on Ca^{2+} transients of embryonic chicken and neonatal rat cardiac myocytes. *J Physiol* **528:**53–63.

David G, Barrett JN, and Barrett EF (1998) Evidence that mitochondria buffer physiological Ca^{2+} loads in lizard motor nerve terminals. *J Physiol* **509:**59–65.

David G, Talbot J, and Barrett EF (2003) Quantitative estimate of mitochondrial $[Ca^{2+}]$ in stimulated motor nerve terminals. *Cell Calcium* **33:**197–206.

Duchen MR, Surin A, and Jacobson J (2003) Imaging mitochondrial function in intact cells. *Methods Enzymol* **361:**353–389.

Dykens JA (1994) Isolated cerebral and cerebellar mitochondria produce free radicals when exposed to elevated Ca^{2+} and Na^+: implications for neurodegeneration. *J Neurochem* **63:**584–591.

Feeney CJ, Pennefather PS, and Gyulkhandanyan AV (2003) A cuvette-based fluorometric analysis of mitochondrial membrane potential measured in cultured astrocyte monolayers. *J Neurosci Methods* **30:**13–25.

Fill M and Copello JA (2002) Ryanodine receptor calcium release channels. *Physiol Rev* **82:**893–922.

Grynkiewicz G, Poenie M, and Tsien RY (1985) A new generation of Ca^{2+} indicators with greatly improved fluorescence properties. *J Biol Chem* **260:**3440–3450.

Gunter KK and Gunter TE (1994) Transport of calcium by mitochondria. *J Bioenerg Biomembr* **26:**471–485.

Gurney ME, Pu H, Chiu AY, Dal Canto MC, Polchow CY, Alexander DD, Caliendo J, Hentati A, Kwon YW, and Deng HX (1994) Motor neuron degeneration in mice that express a human Cu, Zn superoxide dismutase. *Science* **264:**1772–1775.
Herrington J, Park YB, Babcock DF, and Hille B (1996) Dominant role of mitochondria in clearance of large Ca^{2+} loads from rat adrenal chromaffin cells. *Neuron* **16:**219–228.
Hoyaux D, Alao J, Fuchs J, Kiss R, Keller B, Heizmann CW, Pochet R, and Frermann D (2000) S100A6, a calcium- and zinc-binding protein, is overexpressed in SOD1 mutant mice, a model for amyotrophic lateral sclerosis. *Biochim Biophys Acta* **1498:**264–272.
Jaiswal MK, Stefan H, Balakrishnan S, Schomburg E and Keller BU (2006) Disruptions of $[Ca]_i$ and mitochondria in the adult SOD1^{G93A} mouse model of ALS: evidence from recordings in vitro and in vivo. *Soc Neurosci Abstr* **32:**508.8
Kanno T, Fujita H, Muranaka S, Yano H, Utsumi T, Yoshioka T, Inoue M, and Utsumi K (2002) Mitochondrial swelling and cytochrome c release: sensitivity to cyclosporin A and calcium. *Physiol Chem Phys Med NMR* **34:**91–102.
Kong J and Xu Z (1998) Massive mitochondrial degeneration in motor neurons triggers the onset of amyotrophic lateral sclerosis in mice expressing a mutant SOD1. *J Neurosci* **18:**3241–3250.
Ladewig T and Keller BU (2000) Simultaneous patch-clamp recording and calcium imaging in a rhythmically active neuronal network in the brainstem slice preparation from mouse. *Pflugers Arch* **440:**322–332.
Ladewig T, Kloppenburg P, Lalley PM, Zipfel WR, Webb WW, and Keller BU (2003) Spatial profiles of store-dependent calcium release in motoneurones of the nucleus hypoglossus from newborn mouse. *J Physiol* **547:**775–787.
Lips MB and Keller BU (1998) Endogenous calcium buffering in motoneurones of the nucleus hypoglossus from mouse. *J Physiol* **511:**105–117.
Lips MB and Keller BU (1999) Activity-related calcium dynamics in motoneurons of the nucleus hypoglossus from mouse. *J Neurophysiol* **82:**2936–2946.
Mattiazzi M, D'Aurelio M, Gajewski CD, Martushova K, Kiaei M, Beal MF, and Manfredi G (2002) Mutated human SOD1 causes dysfunction of oxidative phosphorylation in mitochondria of transgenic mice. *J Biol Chem* **277:**29626–29633.
Menzies FM, Cookson MR, Taylor RW, Turnbull DM, Chrzanowska-Lightowlers ZM, Dong L, Figlewicz DA, and Shaw PJ (2002a) Mitochondrial dysfunction in a cell culture model of familial amyotrophic lateral sclerosis. *Brain* **125:**1522–1533.
Menzies FM, Ince PG, and Shaw PJ (2002b) Mitochondrial involvement in amyotrophic lateral sclerosis. *Neurochem Int* **40:**543–551.
Mostafapour SP, Lachica EA, and Rubel EW (1997) Mitochondrial regulation of calcium in the avian cochlear nucleus. *J Neurophysiol* **78:**1928–1934.
Murayama T, Kurebayashi N, and Ogawa Y (2000) Role of Mg^{2+} in Ca^{2+}-induced Ca^{2+} release through ryanodine receptors of frog skeletal muscle: modulations by adenine nucleotides and caffeine. *Biophys J* **78:**1810–1824.
Paschen W and Mengesdorf T (2005) Endoplasmic reticulum stress response and neurodegeneration. *Cell Calcium* **38:**409–415.
Pivovarova NB, Hongpaisan J, Andrews SB, and Friel DD (1999) Depolarization-induced mitochondrial Ca^{2+} accumulation in sympathetic neurons: spatial and temporal characteristics. *J Neurosci* **19:**6372–6384.
Ramirez JM, Quellmalz UJ, and Wilken JB (1997) Developmental changes in the hypoxic response of the hypoglossus respiratory motor output in vivo. *J Neurophysiol* **78:**383–392.
Rosen DR, Siddique T, Patterson D, Figlewicz DA, Sapp P, Hentati A, Donaldson D, Goto J, O'Regan JP, and Deng HX (1993) Mutations in Cu/Zn superoxide dismutase gene are associated with familial amyotrophic lateral sclerosis. *Nature* **362:**59–62.
Rowland LP and Shneider NA (2001) Amyotrophic Lateral Sclerosis. *N Engl J Med* **344:**1688–1700.
Schinder AF, Olson EC, Spitzer NC, and Montal M (1996) Mitochondrial dysfunction is a primary event in glutamate neurotoxicity. *J Neurosci* **16:**6125–6133.
Sher AA, Hinch R, Noble PJ, Gavaghan DJ, and Noble D (2007) Functional significance of Na^+/Ca^{2+} exchangers co-localization with ryanodine receptors. *Ann N Y Acad Sci* **1099:**215–220.
Shibata N (2001) Transgenic mouse model for familial amyotrophic lateral sclerosis with superoxide dismutase-1 mutation. *Neuropathology* 21:82–92.
Simpson PB and Russell JT (1997). Role of sarcoplasmic/endoplasmic-reticulum Ca^{2+}-ATPases in mediating Ca^{2+} waves and local Ca^{2+}-release microdomains in cultured glia. *Biochem J* **325:**239–247.
Spitzer NC (2006) Electrical activity in early neuronal development. *Nature* **444:**707–712.
Stock D, Leslie AG, and Walker JE (1999) Molecular architecture of the rotary motor in ATP synthase. *Science* **286:**1700–1705.
Swerdlow RH, Parks JK, Cassarino DS, Trimmer PA, Miller SW, Maguire DJ, Sheehan JP, Maguire RS, Pattee G, Juel VC, et al. (1998) Mitochondria in sporadic amyotrophic lateral sclerosis. *Exp Neurol* **153:**135–142.
Toescu EC and Verkhratsky A (2000) Assessment of mitochondrial polarization status in living cells based on analysis of the spatial heterogeneity of rhodamine 123 fluorescence staining. *Pflugers Arch* **440:**941–947.
Trump BF and Berezesky IK (1995) Calcium-mediated cell injury and cell death. *FASEB J* **9:**219–228.
Van Den Bosch L, Schwaller B, Vleminckx V, Meijers B, Stork S, Ruehlicke T, Van Houtte E, Klaassen H, Celio MR, Missiaen L, et al. (2002) Protective effect of parvalbumin on excitotoxic motor neuron death. *Exp Neurol* **174:**150–161.
Vergun O, Votyakova TV, and Reynolds IJ (2003). Spontaneous changes in mitochondrial membrane potential in single isolated brain mitochondria. *Biophys J* **85:**3358–3366.
Vielhaber S, Kunz D, Winkler K, Wiedemann FR, Kirches E, Feistner H, Heinze HJ, Elger CE, Schubert W, and Kunz WS (2000). Mitochondrial DNA abnormalities in skeletal muscle of patients with sporadic amyotrophic lateral sclerosis. *Brain* **123:**1339–1348.
von Lewinski F and Keller BU (2005a) Ca^{2+}, mitochondria and selective motoneuron vulnerability: implications for ALS. *Trends Neurosci* **28:**494–500.
von Lewinski F and Keller BU (2005b) Mitochondrial Ca^{2+} buffering in hypoglossal motoneurons from mouse. *Neurosci Lett* **380:**203–208.
Wei H and Perry DC (1996) Dantrolene is cytoprotective in two models of neuronal cell death. *J Neurochem* **67:**2390–2398.
Wiedemann FR, Manfredi G, Mawrin C, Beal MF, and Schon EA (2002) Mitochondrial DNA and respiratory chain function in spinal cords of ALS patients. *J Neurochem* **80:**616–625.
Wong PC, Pardo CA, Borchelt DR, Lee MK, Copeland NG, Jenkins NA, Sisodia SS, Cleveland DW, and Price DL (1995) An adverse property of a familial ALS-linked SOD1 mutation causes motor neuron disease characterized by vacuolar degeneration of mitochondria. *Neuron* **14:**1105–1116.
Wyatt CN and Buckler KJ (2004) The effect of mitochondrial inhibitors on membrane currents in isolated neonatal rat carotid body type I cells. *J Physiol* **556:**175–191.
Xu K, Tavernarakis N, and Driscoll M (2001) Necrotic cell death in *C. elegans* requires the function of calreticulin and regulators of Ca^{2+} release from the endoplasmic reticulum. *Neuron* **31:**957–971.

Address correspondence to: Dr. Bernhard U. Keller, Center of Physiology, University of Goettingen, Humboldtallee 23, 37073, Goettingen, Germany. E-mail: bkeller1@gwdg.de